Microvascular Research 143 (2022) 104386

Contents lists available at ScienceDirect

Microvascular Research

journal homepage: www.elsevier.com/locate/ymvre

Hierarchical data visualization of experimental erythrocyte aggregation employing cross correlation and optical flow applications

Bruce I. Gaynes [a,b], Mark B. Shapiro [c,d], Abel Saju Augustine [c], Yang Xu [e], Yang Lin [f], Parisa Mirbod [g], Robert S. Dieter [a,b], Yang Cheng [h], Mengren Wu [g], Harish Venkataraman [i], Yuan Gao [g], Plamen Petrov [i,j], Jie Xu [g,*]

[a] Loyola University Chicago, Stritch School of Medicine, Maywood, IL, United States of America
[b] Edward Hines Jr. VA Medical Center, Hines, IL, United States of America
[c] Anthem, Inc., 220 Virginia Ave, Indianapolis, IN 46204, United States of America
[d] University of Illinois at Chicago, Richard and Loan Hill Department of Biomedical Engineering, 851 S Morgan St, Chicago, IL 60607, United States of America
[e] San Diego State University, Department of Computer Science, 5500 Campanile Dr, San Diego, CA 92182, United States of America
[f] University of Rhode Island, Department of Mechanical, Industrial & Systems Engineering, 2 East Alumni Avenue, Kingston, RI 02881, United States of America
[g] University of Illinois at Chicago, Department of Mechanical and Industrial Engineering, 842 W Taylor Street, Chicago, IL 60607, United States of America
[h] University of Southern California, Viterbi Department of Computer Science, 941 Bloom Walk, Los Angeles, CA 90089, United States of America
[i] University of Illinois at Chicago, Department of Computer Science, 851 S Morgan St, Chicago, IL 60607, United States of America
[j] Hydrogen Health, 125 W 25th St, New York, NY 10001, United States of America

ARTICLE INFO

Keywords:
Microfluidics
Erythrocyte
Aggregation
Hemorheology
Cross-correlation

ABSTRACT

Appraisal of microvascular erythrocyte velocity as well as aggregation are critical features of hemorheological assessment. Examination of erythrocyte velocity-aggregate characteristics is critical in assessing disorders associated with coagulopathy. Microvascular erythrocyte velocity can be assessed using various methodologic approaches; however, the shared assessment of erythrocyte velocity and aggregation has not been well described. The purpose of this study therefore is to examine three independent erythrocyte assessment strategies with and without experimentally induced aggregation in order to elucidate appropriate analytic strategy for combined velocity/aggregation assessment applicable to in-vivo capillaroscopy. We employed a hierarchical microfluidic model combined with Bland-Altman analysis to examine agreement between three methodologies to assess erythrocyte velocity appropriate for interpretation of cinematography of in-vivo microvascular hemorheology. We utilized optical and manual techniques as well as a technique which we term transversal temporal cross-correlation (TTC) to observe and measure both erythrocyte velocity and aggregation. In general, optical, manual and TTC agree in estimation of velocity at relatively low flow rate, however with an increase in infusion rate the optical flow method yielded the velocity estimates that were lower than the TTC and manual velocity estimates. We suggest that this difference was due to the fact that slower moving particles close to the channel wall were better illuminated than faster particles deeper in the channel which affected the optical flow analysis. Combined velocity/aggregation appraisal using TTC provides an efficient approach for estimating erythrocyte aggregation appropriate for in-vivo applications. We demonstrated that the optical flow and TTC analyses can be used to estimate erythrocyte velocity and aggregation both in ex-vivo microfluidics laboratory experiments as well as in-vivo recordings. The simplicity of TTC method may be advantageous for developing velocity estimate methods to be used in the clinic. The trade-off is that TTC estimation cannot capture features of the flow based on optical flow analysis of individually tracked particles.

1. Introduction

The use of in-vivo microvascular capillaroscopy has evolved into an accepted method of describing the intravascular milieu from both hemorheological and microangiopathic perspectives. Disorders such as stroke and various forms of coagulopathy such as that related to COVID-

* Corresponding author.
E-mail address: jiexu@uic.edu (J. Xu).

https://doi.org/10.1016/j.mvr.2022.104386
Received 28 January 2022; Received in revised form 28 April 2022; Accepted 19 May 2022
Available online 24 May 2022

19 are strongly correlated with abnormal hemorheological metrics (Renoux et al., 2021; Wagner et al., 2013; Neumann et al., 1991). Historically, in-vivo assessment of erythrocyte passage within the microvascular lumen has been conducted by iterations of a space-time analysis in which erythrocyte location is transformed on a coordinate system then interpreted by evaluation of instantaneous velocity of a single erythrocyte temporally. The resultant output can be represented visually by a series of sloped lines indicating factors such as overall velocity, tube hematocrit and flux (Ellis et al., 1992). While metrics such as erythrocyte velocity and flux provide important hemorheological measures of cardiovascular hemodynamics, the space time analytic approach negates assessment of an important corollary to erythrocyte velocity, namely erythrocytic aggregate metrics and assessment of flow field homogeneity.

A detailed understanding of erythrocyte aggregation is important clinically since aggregation is typically enhanced during pathophysiological processes, including circulatory and metabolic disorders, hematological pathologies and sepsis (Wagner et al., 2013). Importantly, altered erythrocyte aggregation may be an indicator of disease as well as a factor affecting the course of the clinical condition. Indeed, the prognostic value of erythrocyte aggregation indices has been demonstrated in various diseases conditions (Wagner et al., 2013). Erythrocyte aggregation induced in the presence of plasma macromolecules or in experimental model systems through use of dextran polymers is clinically termed “rouleaux.” Due to the low intercellular attractive forces rouleaux bonds are relatively weak, thus shear force alone can easily break up the rouleaux into individual erythrocytes leading to a pronounced shear induced thinning of blood and reduction in blood viscosity (Wagner et al., 2013).

From a hemorheological perspective, prior studies have suggested that assessment of erythrocyte velocity without consideration of flow field composition characterized by shear-induced viscosity, erythrocyte deformability and flow field homogeneity has uncertain clinical value (De Backer et al., 2007; Kaliviotis et al., 2016; Passos et al., 2019). Homogeneity of the microvascular flow field is an important feature of the microvascular milieu and is thought to improve tissue oxygenation as well as reduce the likelihood of endothelial injury (De Backer et al., 2007). Accordingly, a sluggish, homogenous low flow may be better tolerated than a heterogenous high flow, even when total blood flow is lower (Ellis et al., 2002). Identification of “sluggish” flow is considered to be a product of erythrocyte aggregation and shear, the latter being a modifying factor in microvascular viscosity. The most common method for capillary red blood cell tracking is based on spatiotemporal image (STI) analysis (Ellis et al., 1992; Koutsiaris et al., 2010). Although current space-time analysis modalities provide metrics for velocity and identify flux and cell packing (Ellis et al., 1992) from a signal processing perspective space-time analysis does not fully describe interaction and correspondence of signal features temporally. An alternative analytic approach that optimizes assessment of erythrocyte aggregation and benefits identification of homogeneity in the fluid space would be desirable, in other words, optimizing identification of erythrocyte aggregates as signals applicable to data streaming and pattern recognition. Cross-correlation is such a signal processing paradigm that essentially measures similarity of two series as a function of the displacement of one relative to the other (Yuan and Mills, 2005). Cross-correlation is useful for determining the time delay between two signals, e.g., for determining time delays for the propagation of signals across a particular array (Yuan and Mills, 2005). Further, cross-correlation is amenable to pairing with procedures such as principal component analysis in a manner that aids identification of noise factors in the flow field (Scherl et al., 2020). Thus, using cross-correlation one can assess uniformity of erythrocyte characteristics temporally in both a quantitative and qualitative manner. Greater uniformity in cross-correlation signal strength is consistent with greater homogeneity in the flow field and thus may better differentiate sluggish homogenous flow from rapid heterogenous flow. Visual interpretation of cross-correlation values as a heatmap matrix can also provide important visualization clues of how erythrocyte clustering and heterogeneity varies over space and time. Based on the notion of the importance of assessing erythrocyte aggregation and microvascular flow homogeneity, the value of cross-correlation as an alternative to space-time analysis becomes highly relevant. The purpose of this study is therefore to demonstrate the application of cross-correlation methods to interpretation of experimentally induced erythrocyte aggregation as a metric of fluid field homogeneity (Yuan and Mills, 2005).

2. Methods

2.1. Experimental setup

The microchannel used in this experiment was built on a commercial linear microfluidic chip (thin XXS LCS0109, IDEX Health & Science, Germany), which consists of a square channel with cross-sectional area of 50 μm by 50 μm. To mimic blood flow, a syringe pump (Nexus 3000, CHEMYX, United States) was connected with the microfluidic channel through a tube to load the blood sample. The device was mounted on the stage of an inverted microscope system (Nikon Eclipse Ti-S, Nikon Instruments Inc., Japan) and the flow motion of the sample were observed and recorded using a high-speed camera (Phantom Miro M310, Vision Research Inc., United States). We analyzed the microfluidic flow videos for the 50 × 50 μm channel. The videos depict flow under three different syringe pump setting conditions which are three infusion rates of 0.045 μl/min, 0.06 μl/min, and 0.075 μl/min. The three same conditions are further applied on blood flow with or without added dextran. To obtain the high-quality image sequence, the capturing resolution and frame rate was set up as 1280 × 720 and 60 fps, respectively.

2.2. Sample preparation

Porcine whole blood (Innovative Research, United States) was anticoagulated by heparin solution. To simulate blood flow with and without erythrocyte aggregation, two groups of samples were prepared. In erythrocyte aggregation group, the dextran-PBS solution was prepared by mixing dextran with 1× phosphate buffer solution (PBS 1×, Corning, United States). The dextran used in this experiment is Dx 500 molecular weight (31392 Sigma-Aldrich, United States). The dextran was diluted with PBS to achieve a final concentration of 2.5% (Renoux et al., 2021). Afterwards, the whole blood samples were mixed with dextran solution, which consists of 6.25% blood + 93.75% dextran PBS solution. To compare the effect of aggregation on blood flow, the group without erythrocyte aggregation was prepared by diluting whole blood with PBS solution at the same dilution ratio, which consists of 6.25% blood + 93.75% 1× PBS solution. The hematocrit was considered equivalent in both with and without dextran cases, as the dilution ratio was equal in both experimental settings.

3. Microfluidics experiments

3.1. Estimation of particle velocity and particle aggregation

First, we enhanced contrast of the videos using adaptive thresholding (Fig. 1). We then estimated the erythrocyte velocity and aggregation based on cross-correlation of the time series of pixel intensity in a grid of transversal cross-sections superimposed on each video frame (Fig. 1). We call this method transversal temporal cross correlation (TTC) in the remainder of the paper.

The TTC analysis was performed as follows. First, we selected a segment of video with clearly visible flow. We then superimposed a grid of equally spaced lines, or cross-sections, perpendicular to the channel walls (grey vertical lines in Fig. 1). For each frame, we measured the average pixel density across each cross-section. Erythrocytes appear as dark spots (Fig. 1), and when an erythrocyte crosses a cross-section, it

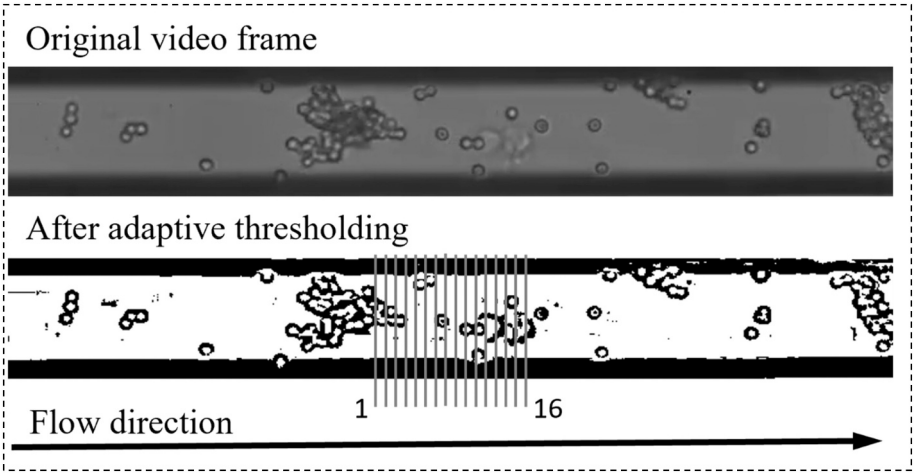

Fig. 1. A frame in a 50 × 50 μm channel video with sixteen cross-sections. The distance between the cross-sections was 17.2 pixels, equivalent to 7.9 μm.

reduces the pixel intensity of that part of the cross-section. If erythrocytes do not form clumps, then the average intensity across a cross-section is not expected to vary by much because a single cell is small compared with the channel width, and a large number of erythrocytes is not expected to cover a cross-section at any given time. Conversely, if a clump of erythrocytes moves through a cross-section, then the pixel intensity of a large portion of the cross-section decreases which should be reflected in a transient decrease in the average intensity. For each cross-section shown in Fig. 1, for a series of frames we obtained a time series of average intensity, with frame number as proxy for time (Fig. 2). A large dip in this time series reflects a clamp moving through the cross-section. If a clump does not break up while moving through several consecutive cross-sections, it produces another dip in the intensity time series evaluated for the next cross-section downstream, then the third cross-section, and so on until it breaks up. The dip in each subsequent time series will be shifted by several frames that it takes the clamp to move from one cross-section to the next. This is the key idea behind our TTC method.

When the flow is clumpy, as shown in Fig. 1, the time series for a given cross-section exhibits a pattern of transient dips in average intensity as clumps move across this cross-section (Fig. 2). If these clumps persist while moving across a number of cross-sections then a similar pattern of dips would be present in several time series. For the adjacent cross-sections, this pattern would be shifted by several frames. For a steady flow, the shift is expected to be similar for each pair of adjacent cross-sections. Therefore, it is possible to estimate the velocity of clumpy flow based on a shift of the patterns of dips in the average intensity time series for the adjacent cross-sections.

The shift in the dip pattern in the time series for a pair of cross-sections was estimated using cross correlation analysis of the corresponding pair of time series. We calculated sample Pearson correlation coefficients between the time series for each pair of cross-sections 1–2, 2–3, 3–4, etc. (Fig. 3A and Table 1). Each point in the plots in Fig. 3A is a correlation coefficient for a given pair of time series. The first time series $X(i)$ is taken as is, the second time series is either not shifted, or shifted a number of frames K forward (positive lag K) or backward K (negative lag K), denoted as $Y(i - K)$. We then calculated Pearson cross-correlation coefficients $r(K)$ for a range of lags K from −16 to +5 (Fig. 3A). When the second time series $Y(i - K)$, that corresponds to a cross-section downstream, is shifted back by some K^* such that the patterns of dips overlap the most, the correlation coefficient $r(K^*)$ is expected to be the highest. Therefore, the lag K^* of the peak in the cross-correlation plot in Fig. 3A indicates the number of frames that would take for clumps to move across this pair of cross-sections. The clump velocity is calculated

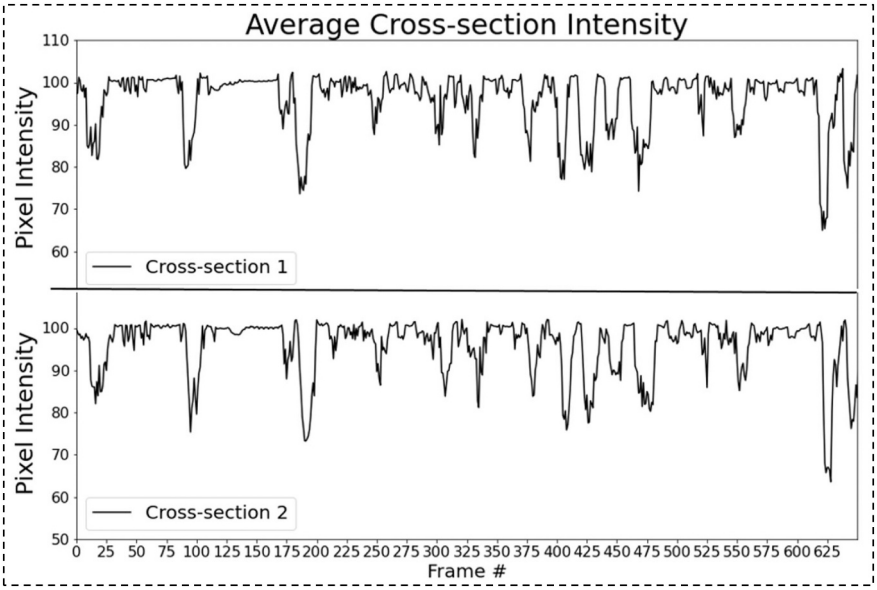

Fig. 2. Time series of the mean of the pixel intensities for cross-sections 1 and 2. The time series for cross-section 2 lags the one for cross-section 1 by several frames.

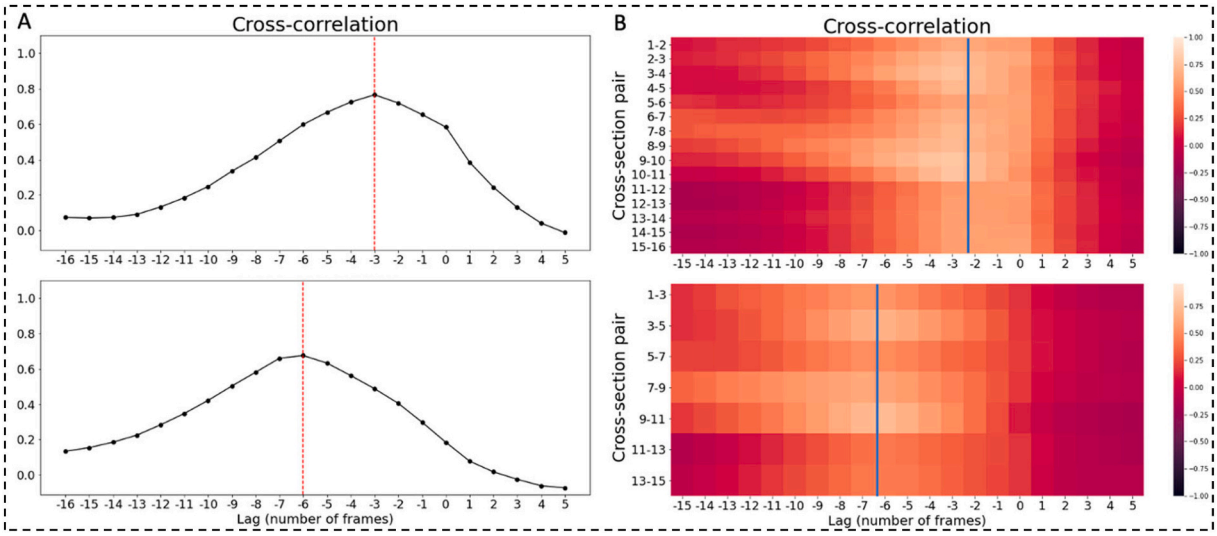

Fig. 3. A. Cross-correlation between the average intensity time series for cross-sections 1–2 (top) and 1–3 (bottom). The vertical line indicates the lag of the peak of cross-correlation. As the distance between the cross-sections doubles the lag also doubles from −3 (top) to −6 (bottom), as expected. B. The cross-correlation for all adjacent cross-section pairs (top) and pairs two spaces apart (bottom), shown as a heatmap. Each row corresponds to a cross-correlation lag series for one pair of cross-sections. The vertical lines indicate the average lag of the cross-correlation peak for all cross-section pairs.

Table 1
Velocity estimates for microfluidic experiments. Four videos (denoted as video index) were recorded for each flow rate condition.

Conditions	Video index	Manual estimate (mm/s)	Optical flow estimate (mm/s)	TTC estimate (mm/s)	Peak cross-correlation
With dextran					
1	1	0.137	0.136	0.154	0.78
	2	0.148	0.142	0.162	0.72
	3	0.156	0.159	0.184	0.66
	4	0.188	0.167	0.202	0.74
	Average (SD)	0.157 (0.022)	0.151 (0.014)	0.175 (0.022)	
2	1	0.231	0.181	0.218	0.57
	2	0.220	0.191	0.219	0.68
	3	0.218	0.187	0.235	0.66
	4	0.252	0.214	0.285	0.57
	Average (SD)	0.230 (0.016)	0.193 (0.014)	0.239 (0.031)	
3	1	0.314	0.233	0.289	0.57
	2	0.356	0.237	0.352	0.57
	3	0.316	0.245	0.320	0.51
	4	0.345	0.248	0.359	0.54
	Average (SD)	0.333 (0.021)	0.241 (0.007)	0.330 (0.032)	
No dextran					
1	1	0.071	0.102	0.092	0.10
	2	0.077	0.103	0.084	0.10
	3	0.066	0.101	0.100	0.10
	4	0.077	0.097	0.082	0.10
	Average (SD)	0.073 (0.005)	0.101 (0.002)	0.090 (0.007)	
2	1	0.354	0.258	0.357	0.26
	2	0.274	0.247	0.400	0.25
	3	0.259	0.237	0.366	0.24
	4	0.265	0.255	0.412	0.26
	Average (SD)	0.288 (0.044)	0.249 (0.009)	0.384 (0.026)	
3	1	0.504	0.338	0.457	0.34
	2	0.489	0.332	0.441	0.33
	3	0.476	0.367	0.403	0.37
	4	0.606	0.367	0.577	0.37
	Average (SD)	0.519 (0.059)	0.351 (0.019)	0.470 (0.075)	

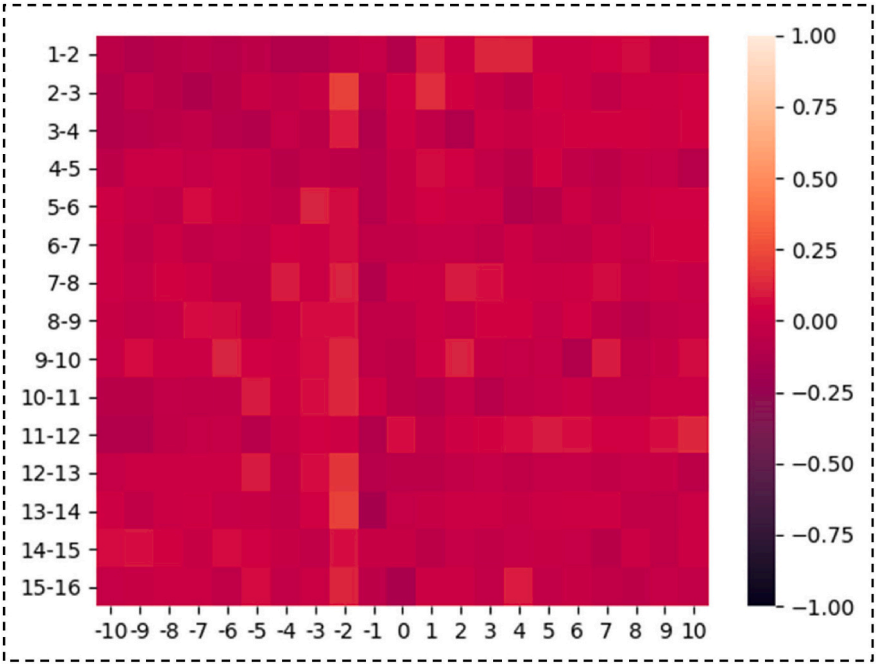

Fig. 4. Cross-correlation heatmap for the 50 × 50 μm channel video without dextran. The low cross-correlation reflects the absence of particle aggregation.

given lag K^*, frame rate, and distance between the cross-sections. Moreover, a greater erythrocyte aggregation is expected to produce more pronounced pattern of dips in average intensity and consequently a higher cross-correlation peak $r(K^*)$.

We estimated the particle velocity for the whole channel by looking at the position of the peaks of cross-correlations for all pairs of cross-sections. A convenient way to conduct this task is to represent the cross-correlation plots as a heatmap (Fig. 3B). For each row of the heatmap matrix, we determined the number of frames that corresponded to the cross-correlation peak. We then averaged the number of frames across all rows, i.e., cross-section pairs, and also averaged the corresponding values of the cross-correlation peaks. We then converted the number of frames into the time lag and then estimated the particle velocity for the whole channel given the distance between the cross-sections. We assigned the averaged value of the cross-correlation peaks to that particular condition (Table 1).

In this experiment, erythrocyte aggregates typically underwent disruption and reformation as the cells move through the channel. If the grid spacing between the cross-section is too large then the clumps would break up before reaching the next cross-section, and the cross-correlation would not reflect the clumpy flow. On the other hand, if the spacing is too small then it would take very few frames for a clump to move from one cross-section to another which limits the temporal resolution of the method. The best spacing depends on the interplay between the clump persistence and velocity and is not known a priori. Therefore, we repeated the cross-correlation analysis for different spacing between the cross-sections. Specifically, we calculated the cross-correlation for the adjacent cross-sections, and then repeated the analysis for cross-sections further apart 1–3, 3–5, 5–7, etc., and 1–4, 4–7, 7–10, etc. The spacing that produced the highest cross-correlation peaks across all pairs was used for velocity estimation.

The TTC method can be also used to estimate particle velocity if particles do not aggregate. In this case, the cross-correlation values are low, as we observed in experimental conditions without dextran (Fig. 4).

3.2. Optical flow method

Optical flow is the pattern of apparent motion of image objects between two consecutive frames caused by the movement of objects (or camera) in a video. An optical flow algorithm can estimate a two-dimensional (2D) vector field, where each vector measures the movement from the previous frame to the next. There are two optical flow algorithms that are commonly implemented in computer vision software packages, the *Lucas-Kanade* method and the *dense* method (a.k.a., Gunnar Farnebäck's algorithm) (Farnebäck, 2003). The generic optical flow method assumes that the pixel intensities of an object do not change between consecutive frames, and that the neighboring pixels have similar motions (indicated by Eq. (1)). From these assumptions, we derived a derivative equation, termed "optical flow" equation (Eq. (2)). The f in Eq. (2) is the gradient of pixel intensity of an image. The subscript indicates the dimension along which the gradient is computed, that is, f_x is the gradient along x-axis, f_y is along y axis, and f_t is along the

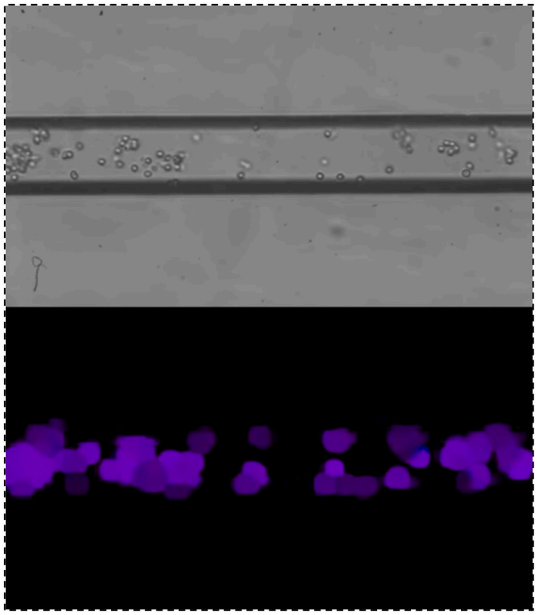

Fig. 5. A snapshot for the microfluidics experiment with dextran (top). The corresponding dense optical visualized output (bottom).

time. The u and v in Eq. (2) denote the movements per unit time, i.e., velocities, along the x- and y-axes, and they are the target variables to be estimated.

$$I(x, y, t) = I(x + dx, y + dy, t + dt) \tag{1}$$

$$f_x u + f_y v + f_t = 0, \text{where } f_x = \frac{\partial f}{\partial x}; f_y = \frac{\partial f}{\partial y}; u = \frac{\partial x}{\partial t}; v = \frac{\partial y}{\partial t} \tag{2}$$

Different algorithms estimate u and v in different ways. Lucas-Kanade converts Eq. (2) to a solvable form using least square fit method, which is essentially equivalent to a Harris corner detection operator. Therefore, the performance of this method is constrained by the degrees to which corners, i.e., the junction of edges, can be successfully detected. Because edges are detected by sudden change in image brightness, this method often fails when the camera resolution is insufficient or the lighting condition is suboptimal.

To overcome the limit of Lucas-Kanade method, we used the dense method in this study. This method does not require the usage of corner detector, but rather it computes the optical flow for all points in the frame. Given two adjacent frames in a video, the algorithm returns the magnitude and direction of velocity for each pixel point. The magnitude is our primary focus here. We use m_ij to denote the velocity magnitude for the pixel point located at position (i, j) ($0 < i < H$ and $0 < j < W$; H and W are the height and width of a frame). Then we compute the gross average of all magnitude values within one frame:

$$\frac{1}{H^* W} \sum_i \sum_j m_{ij} \tag{3}$$

Due to the high sensitivity of the dense optical flow (Fig. 5), it computes and returns a magnitude value for any moving pixel points, no matter how large/small the moving distance is. However, among these returned magnitude values, not all of them correspond to the actual movement of blood cells of our interest. Therefore, we removed the pixels where the velocity magnitude is 2 times the standard deviation away from the mean value, which is a basic empirical rule in statistics (Pukelsheim, 1994).

Owing to the fact that infusion rates might non-uniformly impact the velocity of RBCs, we devised a method to measure velocity of the particles by manually tracking the particles on a frame-by-frame basis along the length of the microchannel (manual estimation method). We recorded the number of frames that it took for the particles to move between cross-sections and use the methods outlined in the cross-correlation section to derive the velocity. The number of frames that is found manually along with the velocity derived from this type of tracking the third velocity estimate against which we compared the TTC and optical flow methods.

3.3. In-vivo video

High definition capillaroscopy of the conjunctival microcirculation was obtained from subjects presenting for ophthalmic examination at the Edward Hines Jr. VA Medical Center. In-vivo microvascular imaging was approved by the Edward Hines Jr. VA Medical Center institutional review board and complied with the tenets of the Declaration of Helsinki. Informed consent was received from all subjects prior to imaging.

Using a commercially available capillaroscopic camera (CapiScope^{tm} KK Technology, Devon England), video of conjunctival venular microvascular flow was recorded and utilized for off-line analysis using methodology previously described in Sections 3.1 and 3.2 of this study. The CapiSCope is a hand-held device previously evaluated by the FDA and deemed a minimal risk device for capillaroscopic examination of the conjunctival microvasculature. The CapiScope camera system employs orthogonal polarization spectral (OPS) imaging that allows for non-invasive evaluation and quantification of the human microcirculation in vivo. In this technique, cross polarization of reflected green light results in the enhancement of the contrast of vascular structures in a hemoglobin dependent manner.

4. Results

4.1. With vs without dextran analysis

For the videos containing flow with dextran, aggregation is clearly visible in the videos, and hence there are pronounced patterns in the time series for any cross-section. For all the experiments with dextran, the average cross-correlation peak was at least above 0.2 which can be interpreted as the flow patterns being picked up across different cross-sections along the channel (Fig. 6). Consequently, this gives us a reliable measurement of velocity from cross-correlation, which is in good agreement with the velocity derived from manual estimation.

In the case of without dextran, there is no aggregation, however the TTC method still allowed us to obtain estimates of the particle velocity that were in good agreement with the manual estimation method (Table 1, also Fig. 7).

4.2. Comparison between the methodologies

We used Bland-Altman plots to compare the estimates of particle

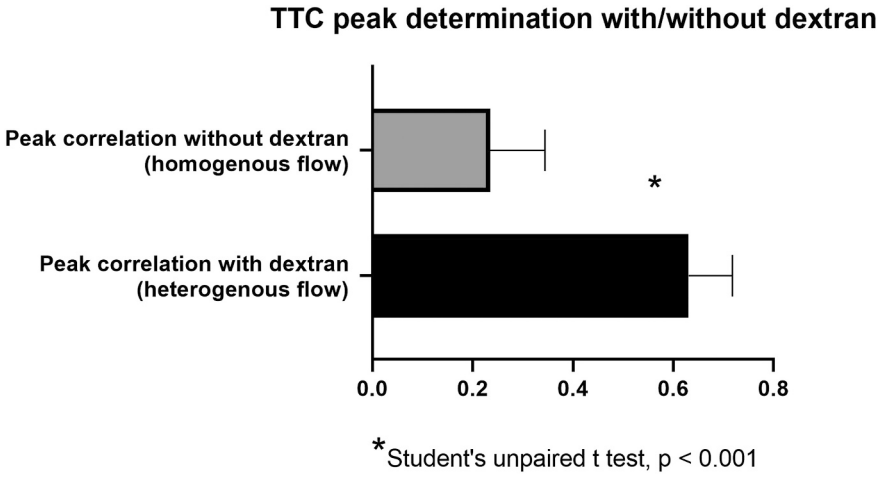

Fig. 6. The peak cross-correlation returned the TTC method provided a criterion to assess erythrocyte aggregation. Adding dextran to the porcine blood induced aggregation that was reflected in the peak cross-correlation consistently higher than 0.2 and statistically significantly higher than the peak cross-correlation in the experiments without dextran.

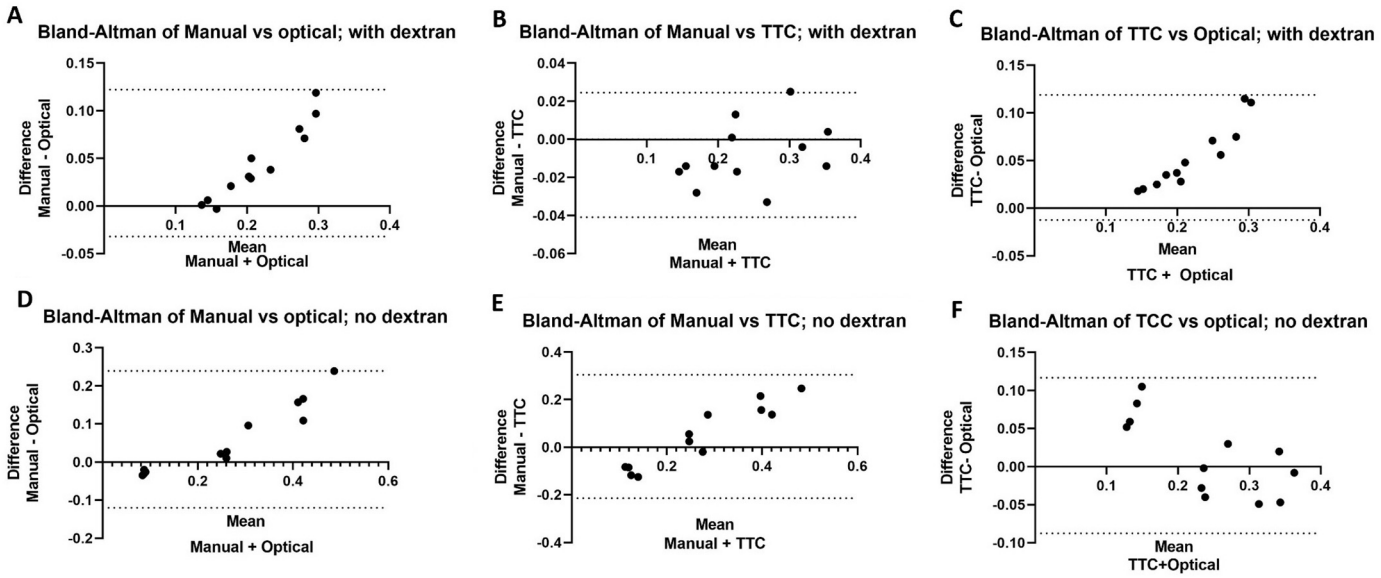

Fig. 7. Bland-Altman plots comparing measurement techniques. Substantial bias is seen with manual vs optical (panel A) and TTC vs optical (panel C) measurement techniques with added dextran. Manual vs TTC (panel B) velocity estimates with dextran are uniformly heterogenous across all values of mean velocity. Manual velocity measurement conditions without dextran demonstrated bias toward higher velocity estimation as mean velocity increased (panels D, E). In contrast, TTC vs optical assessment methods without dextran demonstrate approximate uniformity with escalating mean velocity (panel F). The 95% limit of agreement is denoted by the upper and lower dotted lines in each plot.

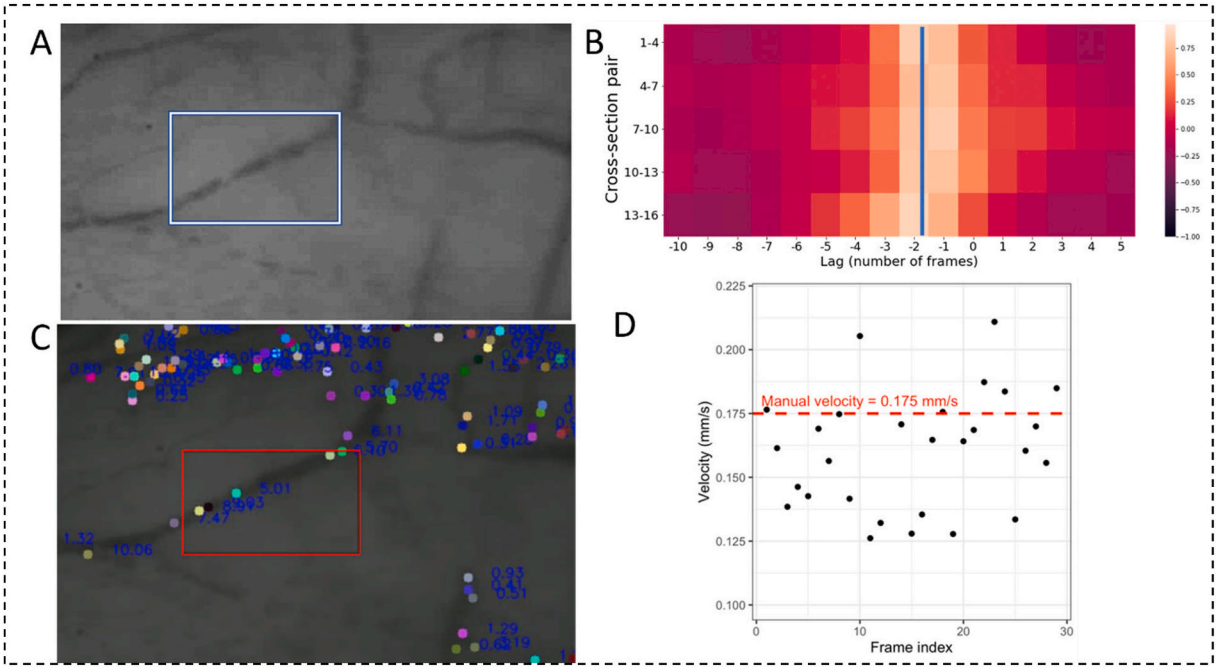

Fig. 8. A. In-vivo video frame with a region that contained the blood vessel of interest. B. Cross-correlation heatmap, vertical line shows the average lag of the cross-correlation peak at −1.6 frames. C. The in-vivo video frame with particle tracking. D. Estimated velocities of individual particles.

velocity across the 50 × 50 μm channel in blood samples with and without dextran. As seen in Fig. 7, optical flow analysis estimates diverged from both the TTC and manual estimates as the velocity increased with the flow rate. One possible explanation of this effect is that the optical flow algorithm better detects the brighter lit particles that are closer to the transparent channel wall than the particles moving deeper in the channel. Multiple studies showed that particles in the center of a microfluidics channel are moving faster than those close to the wall (Stergiou et al., 2019). Because the method we used to calculate the overall optical flow velocity is to include the vast majority of pixels in the video frame, which includes the near-wall pixel points that have lower velocity values and other noisy data points due to the algorithm accuracy. As a result, it smooths the final velocity values and makes them less various to flow rate. To overcome this issue, an accurate method of determining the center vs near-wall area in the video frame, and of filtering out noisy pixel points need to be developed in future investigation. The TTC method evaluates the overall intensity across each cross-section and is likely less sensitive to that difference in the velocity of particles in the center vs close to the channel wall. For the manual estimation, we subjectively picked a particle or a cluster of

particles that was somewhat "representative" of the overall flow and traced it across a number of frames. Doing manual velocity estimate for many particles would involve considerable effort and was beyond the scope of this paper. Assessment of Bland-Altman plots of the velocity profiles clearly portrays bias in velocity measurement techniques in an illustrative manner as denoted in Fig. 7.

4.3. Exploratory results on in-vivo video

We tested the applicability of TTC, optical and the manual methods of velocity analysis on a video of in-vivo blood vessels. The video had a duration of 2.10 s, a resolution of 638 × 370 pixels, and a frame rate of 60 FPS. The video was selected among a large set of candidate videos, because it contained segments with satisfactory stability and sharpness. The video was further stabilized by selecting a suitable segment, cutting out the main area of interest, and applying a video stabilization algorithm implemented in Python.

We cropped a region within the original video to focus on the main vessel (Fig. 8A), and applied the TTC, optical flow, and manual analyses to that region. The manual velocity estimate was 0.175 mm/s. The cross-correlation heatmap exhibited high cross-correlation (Fig. 8B). We estimated the erythrocyte velocity using cross-sections 1–4, 4–7, etc., that provided a reasonable distance to estimate the lag of 1.6 frames or 0.52 s that yields a velocity estimate of 0.153 mm/s, peak cross-correlation 0.87.

As shown in Fig. 8C, the flowing blood cells can be detected by the optical flow algorithm, which are indicated by the colored dots, and the raw velocities of the those moving dots are computed as well (see the numbers attached to each dot). Note that, these velocity values are unscaled ones, and the unit is pixel/s. We validate the computed optical flow velocities with the following two methods. First, we use the same manual method as in previous section to measure the pixel velocity within the box region, and compare to the optical flow results. Second, we extract the optical velocity for each frame (Fig. 8D). The manual velocity value is plotted as the horizontal line at 0.175 mm/s, which is close to the mean value of optical flow velocity of 0.160 mm/s.

Using a 2-way ANOVA, the interaction between method of velocity determination and infusion rate was examined for both dextran and non-dextran conditions. For the dextran conditions, the method of analysis accounts for 12.44% of the total variance in velocity measurement while the infusion rate accounted for 80.75% ($p < 0.001$). For the non-dextran conditions, the method accounted for 4.55% of the variance in velocity assessment while the infusion rate accounted for 87.6% of the total variance ($p < 0.001$). Clearly factors aside from methodology and infusion rate impacts velocity assessment in manner that may be detectable by scrutiny of erythrocyte cell-cell interaction as well as interaction with various plasma immunoglobulins.

Overall, the results from in-vivo video analysis suggests that both the TTC and optical flow methods can generate stable and accurate measures on blood flow rate, which is consistent with the ex-vivo experiments in previous sections. This is positive evidence for further applications of these methods to clinically relevant studies that involve in-vivo recordings of the capillary flow in the eye conjunctiva.

5. Discussion

Vascular flow models typically assume that blood is a continuous fluid and its particulate nature is accounted through the definition of effective viscosity. Whole blood is a complex suspension consisting mainly of homogenous plasma proteins and deformable, interacting erythrocytes. The degree of cell–cell interaction depends on many factors such as local flow conditions, flow hematocrit, local vessel geometry, pharmacologic alteration of cell membrane receptors and hemodynamic circumstances of cardiac function (Wagner et al., 2013). Abnormality in cell-cell interaction leads to non-uniform cell clustering resulting in radius-dependent variations in viscosity, as seen in the Fahraeus–Lindqvist effect (Pries and Secomb, 2005). Because of these complexities, measured blood viscosity is typically defined as a quantity averaged over a cross-sectional flow area with the aid of the Poiseuille equation. For this reason, it is called "apparent" viscosity (Pries and Secomb, 2008).

Conventional capillaroscopic instruments typically rely on various iterations of space time analysis to produce metrics of erythrocyte velocity and in conjunction with measured diameter derive measures of flow and shear. In present study, we demonstrate the complexity of in-vivo velocity assessment by denoting the marked interaction effects of pharmacologic alteration of cell-cell membrane interaction on various methods of velocity assessment. Ascertaining "ground truth" of in-in vivo velocity requires an appraisal of non-uniformity in vessel diameter while simultaneously assessing veracity in flux in a manner that provides metrics of aggregation and shear.

Optical technique for analyzing particle image velocimetry data can be applied to RBC patterns (Guo et al., 2013). The technique uses point-by-point illumination of the particle image and two subsequent 2D FFTs are used to produce an autocorrelation pattern of the RBCs from which RBC displacement is determined. This output is amenable to machine learning and AI interpretation of microvascular flow important in assessing factors such as coagulopathy and response to treatment intended to reduce thrombotic events. The TTC and optical flow methods have different advantages and shortcomings that make each method better suited for different scenarios. The optical flow method can be used to study different features of particle movement, including velocity, trajectory, and particle aggregation which paves the way to deeper understanding of fluid mechanics of the blood flow.

The trade-off for high resolution of the optical flow analysis is higher computational complexity compared to cross-correlation methods such as TTC or the spatial-temporal image (STI) analysis proposed by Khansari et al. (2015). The TTC method proposed in this study is also simpler than the STI method. As the first step, the STI analysis requires the image to be partitioned such as to identify the center line of the blood vessel and then add lines that span the vessel diameter and are perpendicular to the center line. The TTC method is similar to STI in that it evaluates the temporal changes in intensity across the lines perpendicular to the vessel walls. However, using cross-correlation of the time series of intensities across a grid of cross-sections makes TTC method less dependent on the image analysis and precise positioning of the cross-lines than STI method.

Our results also reflect the Fahreus effect that occurs because the particles in the center of the channel move faster than the particles closer to the walls and as a result, the RBC concentration is higher in the center of the channel. The optical flow analysis is capable of providing an estimate of the distribution of the particle velocities across the channel width. A larger number of particles in the center of the channel weigh more in calculating the average velocity estimated by the optical flow analysis. This contribution of a larger number of particles with higher velocities will reflect the Fahreus effect in the optical flow analysis. Similarly, the TTC method is more sensitive to a larger concentration of particles spanning the cross-sections, and it is expected to reflect the velocity of the particles more concentrated in the center of the channel according to the Fahreus effect. Thus, the velocity estimates by both the optical flow and TTC methods are expected to reflect the Fahreus effect. We found that the estimated particle velocity in all conditions is higher for the TTC than the optical flow method (Table 1, also Fig. 7, Bland-Altman TTC vs optical flow panel). We hypothesize that the Fahreus effect is more pronounced at higher flow rates. We further suggest that because the optical flow method better detects the brighter particles close to the channel walls the velocity estimated by the optical flow method is lower than the that estimated by the TTC method as the flow rate increases, as can be seen in Fig. 7.

The three methods used in this study can be viewed as a progression from a manual estimation of the velocity of a single particle, subjectively deemed "representative", to the optical flow method applied to multiple

tracked particles, and finally to the TTC aggregate estimate of all particle velocities across the channel. The manual velocity estimate is very labor intensive and can be viewed as a "sanity check". The TTC and optical flow methods provide automated estimate of particle velocity and can be used for both research and clinical practice in a wide range of applications that leverage either high resolution or computational simplicity of these methods.

One of the important parameters in reducing the discrepancies observed between the ex-vivo and in-vivo analysis could be because of the difference in the flow used in this study and the blood flow. It is worth noting that analyzing the rheology of the flow diluted with or without dextran studied here is the subject of our current investigation. The obtained results can then be compared with the blood flow viscosity and rheological properties as have been reported in prior studies (Beris et al., 2021). The model can be then utilized as a tool to analyze erythrocyte aggregation and particle velocity distribution across the vessel as well as shear stress (Mirbod, 2016; Shannon and Mirbod, 2017; Wu and Mirbod, 2018; Haffner and Mirbod, 2020; Kang and Mirbod, 2020; Rosti et al., 2021; Mirbod et al., 2009). Additional extensions of this work will be to investigate the flow instability and clustering of erythrocytes by adding dextran and examining in detail blood flow pressure and velocity profiles experimentally. This research will contribute to our understanding of microvascular in-vivo hemorheology as pertains to cardiovascular disorders and stroke.

Declaration of competing interest

The authors declare that they have no known competing financial interests or personal relationships that could have appeared to influence the work reported in this paper.

Acknowledgement

This research was supported in part by funding from Anthem, Inc.

References

Beris, A.N., et al., 2021. Recent advances in blood rheology: a review. Soft Matter 17, 10591–10613.
De Backer, D., et al., 2007. How to evaluate the microcirculation: report of a round table conference. Crit. Care 11 (5), 1–9.
Ellis, C.G., et al., 1992. Application of image analysis for evaluation of red blood cell dynamics in capillaries. Microvasc. Res. 44 (2), 214–225.
Ellis, C.G., et al., 2002. Effect of a maldistribution of microvascular blood flow on capillary O2 extraction in sepsis. Am. J. Phys. Heart Circ. Phys. 282 (1), H156–H164.
Farnebäck, G., 2003. Two-frame motion estimation based on polynomial expansion. In: Scandinavian Conference on Image Analysis. Springer.
Guo, D., Van de Ven, A.L., Zhou, X., 2013. Red blood cell tracking using optical flow methods. IEEE J. Biomed. Health Inform. 18 (3), 991–998.
Haffner, E.A., Mirbod, P., 2020. Velocity measurements of dilute particulate suspension over and through a porous medium model. Phys. Fluids 32 (8), 083608.
Kaliviotis, E., et al., 2016. Quantifying local characteristics of velocity, aggregation and hematocrit of human erythrocytes in a microchannel flow. Clin. Hemorheol. Microcirc. 63 (2), 123–148.
Kang, C., Mirbod, P., 2020. Shear-induced particle migration of semi-dilute and concentrated brownian suspensions in both poiseuille and circular couette flow. Int. J. Multiphase Flow 126, 103239.
Khansari, M.M., et al., 2015. Automated assessment of hemodynamics in the conjunctival microvasculature network. IEEE Trans. Med. Imaging 35 (2), 605–611.
Koutsiaris, A.G., et al., 2010. Blood velocity pulse quantification in the human conjunctival pre-capillary arterioles. Microvasc. Res. 80 (2), 202–208.
Mirbod, P., 2016. Two-dimensional computational fluid dynamical investigation of particle migration in rotating eccentric cylinders using suspension balance model. Int. J. Multiphase Flow 80, 79–88.
Mirbod, P., Andreopoulos, Y., Weinbaum, S., 2009. On the generation of lift forces in random soft porous media. J. Fluid Mech. 619, 147–166.
Neumann, F., et al., 1991. Increased plasma viscosity and erythrocyte aggregation: indicators of an unfavourable clinical outcome in patients with unstable angina pectoris. Heart 66 (6), 425–430.
Passos, A., et al., 2019. The effect of deformability on the microscale flow behavior of red blood cell suspensions. Phys. Fluids 31 (9), 091903.
Pries, A.R., Secomb, T.W., 2005. Microvascular blood viscosity in vivo and the endothelial surface layer. Am. J. Phys. Heart Circ. Phys. 289 (6), H2657–H2664.
Pries, A.R., Secomb, T.W., 2008. Blood flow in microvascular networks. In: Microcirculation. Elsevier, pp. 3–36.
Pukelsheim, F., 1994. The three sigma rule. Am. Stat. 48 (2), 88–91.
Renoux, C., et al., 2021. Impact of COVID-19 on red blood cell rheology. Br. J. Haematol. 192 (4), e108–e111.
Rosti, M.E., Mirbod, P., Brandt, L., 2021. The impact of porous walls on the rheology of suspensions. Chem. Eng. Sci. 230, 116178.
Scherl, I., et al., 2020. Robust principal component analysis for modal decomposition of corrupt fluid flows. Phys. Rev. Fluids 5 (5), 054401.
Shannon, A.T., Mirbod, P., 2017. Three-dimensional flow patterns in the feto-placental vasculature system of the mouse placenta. Microvasc. Res. 111, 88–95.
Stergiou, Y.G., et al., 2019. Experimental and numerical study of blood flow in μ-vessels: influence of the fahraeus-lindqvist effect. Fluids 4 (3), 143.
Wagner, C., Steffen, P., Svetina, S., 2013. Aggregation of red blood cells: from rouleaux to clot formation. C. R. Phys. 14 (6), 459–469.
Wu, Z., Mirbod, P., 2018. Experimental analysis of the flow near the boundary of random porous media. Phys. Fluids 30 (4), 047103.
Yuan, J., Mills, K., 2005. A cross-correlation-based method for spatial–temporal traffic analysis. Perform. Eval. 61 (2–3), 163–180.